CHEMISTRY OF MATERIALS
Article

Chem. Mater. **2010,** *22,* 4335–4345 4335
DOI:10.1021/cm101499x

Active and Stable Embedded Au@CeO_2 Catalysts for Preferential Oxidation of CO

Matteo Cargnello,[†,‡] Cristina Gentilini,[†,#] Tiziano Montini,[†,‡] Emiliano Fonda,[§] Shareghe Mehraeen,[∥,⊥] Miaofang Chi,[⊗] Miriam Herrera-Collado,[∥] Nigel D. Browning,[∥,⊥] Stefano Polizzi,[○] Lucia Pasquato,*[,†] and Paolo Fornasiero*[,†,‡]

[†]*Department of Chemical Sciences and INSTM, Trieste Unit, and* [‡]*ICCOM-CNR Trieste Research Unit and Center of Excellence for Nanostructured Materials* (*CENMAT*), *University of Trieste, via L. Giorgieri 1, 34127 Trieste, Italy,* [§]*Synchrotron SOLEIL L'Orme des Merisiers, St Aubin BP48, 91192 Gif sur Yvette Cedex, France,* [∥]*Department of Chemical Engineering and Materials Science, University of California, Davis, One Shields Avenue, Davis, California 95616,* [⊥]*Department of Molecular and Cellular Biology, University of California, Davis, One Shields Avenue, Davis, California 95616 and Physical and Life Sciences Directorate, Lawrence Livermore National Laboratory, Livermore, California 94550,* [⊗]*Materials Science Division, Oak Ridge National Laboratory, Oak Ridge, Tennessee, 37830, and* [○]*Department of Physical Chemistry-Laboratory of Electron Microscopy, University of Venice, via Torino 155, 30172 Mestre, Venice, Italy.* [#]*Present address: Department of Materials and Institute of Biomedical Engineering, Imperial College London, South Kensington Campus, SW7 2AZ London, United Kingdom.*

Received May 28, 2010

We present a way to stabilize the Au phase supported on ceria by encapsulation of preformed Au nanoparticles (Au NPs) inside a porous ceria layer. The functionalization of the surface of the nanoparticles with carboxylic groups provides the link between the metal phase and the growing $Ce(OH)_x$ barrier, which is then transformed during calcination to obtain the final Au@CeO_2 materials. The sample with a metal loading of 1 wt % shows good activity under real PReferential OXidation (PROX) conditions and better activity than catalysts of higher metal loadings or prepared through optimized deposition-precipitation methods described in the literature. Under simulated aging, the Au(1 wt %)@CeO_2 sample exhibits minor deactivation, which is mainly associated with the formation of carbonates that can be reversed by a mild regenerative oxidative treatment to fully restore its initial activity. Vice versa, the other catalysts show either the unavoidable reversible carbonate poisoning or the irreversible deactivation due to metal sintering/agglomeration phenomena. A plethora of characterization techniques (CO chemisorption, X-ray diffraction, X-ray absorption spectroscopy, aberration-corrected scanning transmission electron microscopy) has been used to confirm the structure of these catalysts and to identify the underlying phenomena controlling their activity.

Introduction

Gold in the nanoscale regime on high surface area oxide supports has demonstrated its high catalytic activity in many chemical reactions.[1,2] Since the pioneering work of Haruta,[3] an extraordinary number of studies have detailed the features of gold as a heterogeneous catalyst in both gas and liquid phases, and in the form of complexes to catalyze reactions in homogeneous phase.[4] Applications in many areas are developing as, for example, in pollution control,[5] chemical processing,[6] sensors,[7] and fuel cell technology.[8] One of the main advantages of Au in catalysis derives from its high chemoselectivity. For this reason, Au has been extensively studied for the PReferential OXidation of CO in the presence of H_2 (PROX).[9,10] As far as heterogeneous catalysis is concerned, experimental and theoretical studies have outlined that the activity of the catalyst is determined by several factors: the size of the nanoparticles (NPs), their charge, nature and porosity of the support, and the specific metal/support electronic interaction.[11−13]

Different methodologies have been reported for the preparation of supported gold catalysts. The methods fall

*To whom correspondence should be addressed. E-mail: lpasquato@units.it (L.P.), pfornasiero@units.it (P.F.).

(1) Hashmi, A. S. K.; Hutchings, G. J. *Angew. Chem., Int. Ed.* **2006**, *45*, 7896.
(2) Li, Z.; Brouwer, C.; He, C. *Chem. Rev.* **2008**, *108*, 3239.
(3) Haruta, M.; Yamada, N.; Kobayashi, T.; Iijima, S. *J. Catal.* **1989**, *115*, 301.
(4) Gorin, D. J.; Sherry, B. D.; Toste, F. D. *Chem. Rev.* **2008**, *108*, 3351.
(5) Haruta, M. *CATTECH* **2002**, *6*, 102.
(6) Mirkin, C. A.; Letsinger, R. L.; Mucic, R. C.; Storhoff, J. J. *Nature* **1996**, *382*, 607.
(7) Nath, N.; Chilkoti, A. *Anal. Chem.* **2002**, *74*, 504.
(8) Cameron, D.; Holliday, R.; Thompson, D. *J. Power Sources* **2003**, *118*, 298.
(9) Bion, N.; Epron, F.; Mariño, M.; Marino, F.; Duprez, D. *Top. Catal.* **2008**, *51*, 76.
(10) Deng, W.; De Jesus, J.; Saltsburg, H.; Flytzani-Stephanopoulos, M. *Appl. Catal., A* **2005**, *291*, 126.
(11) Fu, Q.; Kudriavtseva, S.; Saltsburg, H.; Flytzani-Stephanopoulos, M. *Chem. Eng. J.* **2003**, *93*, 41.
(12) Cuenya, B. R.; Baeck, S. H.; Jaramillo, T. F.; McFarland, E. W. *J. Am. Chem. Soc.* **2003**, *125*, 12928.
(13) Rossignol, C.; Arrii, S.; Morfin, F.; Piccolo, L.; Caps, V.; Rousset, J. L. *J. Catal.* **2005**, *230*, 476.

Published on Web 06/22/2010

into three classes: (i) impregnation of the gold precursor or gold NPs on the preformed support by different methodologies (e.g., incipient wetness, wet impregnation, ion exchange);[14] (ii) contemporary formation of the gold NPs and the support in a single chemical reaction;[14] (iii) building of the support around preformed NPs.[15] Concerning the last approach, a decisive contribution has been given by Corma and co-workers, who developed a route to SiO_2-encapsulated Au NPs.[15] Although this material showed high activity for CO oxidation and good thermal stability after calcination in air, no studies addressed either the PROX reaction or the thermal stability under reaction conditions.

The embedding of NPs in the selected support can not only stabilize the metal phase against sintering but also gives rise to novel properties because of the different and increased interaction between the surface of the NPs and the support.[16] Indeed, simple geometrical considerations suggest that this is a way to maximize the contact area between metal NPs and support, in particular if the size of the cavity is in the range of the NPs' size. For example, ceria appears to stabilize $Au^{\delta+}$ species[17] and to enhance their charge by a redox process that involves oxidation of Au^0 to $Au^{\delta+}$ and reduction of CeO_2 to CeO_{2-x} likely occurring on gold atoms on the surface of the NP and in proximity to the ceria. Another important effect is the cooperativity between gold and ceria, with surface gold atoms in direct contact with ceria being suggested as the most active species for CO oxidation.[18]

The size of the gold particles is a very important parameter in obtaining active catalysts.[19−23] For most reactions, catalysts with Au particles size ranging from 2 to 5 nm lead to good activity. However, catalysts with Au clusters < 0.5 nm, but not dispersed Au atoms, cause very high activity.[24] This is especially true for oxidation of carbon monoxide[25−28] and for PROX.[8,29] The latter process is of use in the purification of hydrogen streams deriving from reforming reactions for application in Proton-Exchange Membrane (PEM) fuel-cells. In combination with Au and other noble and non-noble metals, ceria (CeO_2) has found many applications in catalysis because of its possibility of reversible release and storage of lattice oxygen.[30] This property, the oxygen storage capacity (OSC), is one of the key features for the success of Au/CeO_2 systems in heterogeneous catalysis.

One of the main drawbacks of ceria-based catalysts is their deactivation with time-on-stream and/or shut-down/restart operations.[9] This is mainly due to two reasons: the formation of carbonate/formate species and the consequent blocking of the active sites, or the sintering of the metal particles.[31] The latter phenomenon is the most problematic since it is an irreversible process. Furthermore, Au has a lower melting temperature (1337 °C) than Pd (1825 °C) or Pt (2045 °C) especially in the nanometric range.[32] Therefore, the mobility of Au particles on the support is higher and their sintering is favorable over that of other noble metals. However, few reports address deactivation tests under realistic PROX conditions, giving some uncertainty to the catalytic results. For examples, Deng et al.,[10] Avgouropoulos et al.[33] and Wang et al.[34] reported on the stability of Au catalysts in the PROX reaction, but the tests were conducted at low reaction temperatures (< 200 °C).

Another important point is to understand how the catalyst regenerates. Regarding the first cause of deactivation, transient species such as carbonates can be removed by a treatment in oxygen. For example, Deng et al.[35] reported the favorable effect of adding oxygen to a Au catalyst used for the Water-Gas Shift-Reaction (WGSR). Oxygen is able to decompose cerium hydroxycarbonate formed under reaction conditions. The doping of CeO_2 with Fe(III), La(III), or Zr(IV) also helps removing carbonates because of the ability of these cations to provide hydroxyl groups that are needed in the catalytic cycle.[9] Similarly, oxygen was used to reactivate Au/CeO_2 based catalysts under PROX conditions.[34]

Some of us have already reported that active Au/CeO_2 catalysts for the PROX reaction can be prepared by depositing thiol-protected Au NPs on CeO_2.[36] In the present paper a different concept is explored to design the catalyst by using a flexible procedure where Au NPs are embedded inside the CeO_2 support ($Au@CeO_2$). Au NPs protected by a mixture of thiolates are used to direct the self-assembly assisted precipitation of $Ce(OH)_x$ species around the preformed particles. After removing the

(14) Luengnaruemitchai, A.; Osuwan, S.; Gulari, E. *Int. J. Hydrogen Energy* **2004**, *29*, 429.
(15) Budroni, G.; Corma, A. *Angew. Chem., Int. Ed.* **2006**, *45*, 3328.
(16) Yeung, C. M. Y.; Tsang, S. C. *J. Phys. Chem. C* **2009**, *113*, 6074.
(17) Meier, D. C.; Lai, X.; Goodman, D. W. Surface Chemistry Of Model Oxide-Supported Metal Catalysts: An Overview Of Gold On Titania. In *Surface Chemistry and Catalysis*; Carley, A. F., Davies, P. R., Hutchings, G. J., Spencer, M. S., Eds.; Kluwer Academic/Plenum Publishers: Norwell, MA, 2002; pp 148−207.
(18) Guzman, J.; Carrettin, S.; Fierro-Gonzalez, J. C.; Hao, Y.; Gates, B. C.; Corma, A. *Angew. Chem., Int. Ed.* **2005**, *44*, 4778.
(19) Harding, C.; Habibpour, V.; Kunz, S.; Farnbacher, A.N.-S.; Heiz, U.; Yoon, B.; Landman, U. *J. Am. Chem. Soc.* **2008**, *131*, 538.
(20) Akita, T.; Lu, P.; Ichikawa, S.; Tanaka, K.; Haruta, M. *Surf. Interface Anal.* **2001**, *31*, 73.
(21) Okazaki, K.; Ichikawa, S.; Maeda, Y.; Haruta, M.; Kohyama, M. *Appl. Catal., A* **2005**, *291*, 45.
(22) Okazaki, K.; Morikawa, Y.; Tanaka, S.; Tanaka, K.; Kohyama, M. *Phys. Rev. B* **2004**, *69*, 235404.
(23) Valden, M.; Lai, X.; Goodman, D. W. *Science* **1998**, *281*, 1647.
(24) Herzing, A. A.; Kiely, C. J.; Carley, A. F.; Landon, P.; Hutchings, G. J. *Science* **2008**, *321*, 1331.
(25) Haruta, M. *Catal. Today* **1997**, *36*, 153.
(26) Kozlov, A. I.; Kozlova, A. P.; Asakura, K.; Matsui, Y.; Kogure, T.; Shido, T.; Iwasawa, Y. *J. Catal.* **2000**, *196*, 56.
(27) Kozlov, A. I.; Kozlova, A. P.; Liu, H.; Iwasawa, Y. *Appl. Catal., A* **1999**, *182*, 9.
(28) Tai, Y.; Yamaguchi, W.; Tajiri, K.; Kageyama, H. *Appl. Catal., A* **2009**, *364*, 143.
(29) Kandoi, S.; Gokhale, A. A.; Grabow, L. C.; Dumesic, J. A.; Mavrikakis, M. *Catal. Lett.* **2004**, *93*, 93.
(30) Trovarelli, A. *Catal. Rev.* **1996**, *38*, 439.
(31) Moreau, F.; Bond, G. C. *Top. Catal.* **2007**, *44*, 95.
(32) Buffat, P.; Borel, J. P. *Phys. Rev. A* **1976**, *13*, 2287.
(33) Avgouropoulos, G.; Ioannides, T.; Papadopoulou, C.; Batista, J.; Hocevar, S.; Matralis, H. K. *Catal. Today* **2002**, *75*, 157.
(34) Wang, H.; Zhu, H.; Qin, Z.; Liang, F.; Wang, G.; Wang, J. *J. Catal.* **2009**, *264*, 154.
(35) Deng, W.; Flytzani-Stephanopoulos, M. *Angew. Chem., Int. Ed.* **2006**, *45*, 2285.
(36) Hickey, N.; Larochette, P. A.; Gentilini, C.; Sordelli, L.; Olivi, L.; Polizzi, S.; Montini, T.; Fornasiero, P.; Pasquato, L.; Graziani, M. *Chem. Mater.* **2007**, *19*, 650.

organic layer by calcination, these materials present very small Au NPs dispersed in nanocrystalline CeO_2, with good activities in the PROX reaction and, remarkably, good thermal stability after aging treatments at relatively high temperatures. By using complementary techniques it is shown that the embedded catalysts maintain the dimension of the original Au particles, despite the fact that some Au is completely buried inside the ceria layer and thus not accessible to the reactants.

The paper is organized as follows. First, the synthetic strategy used to prepare the catalyst(s) is described. Then, the catalytic performances under PROX reaction conditions are reported. Finally, characterization of the catalysts, before and after their use, is explained and discussed in light of the catalytic activity observed. This work is based on a sample containing 1% in weight of Au embedded into ceria. For comparison purposes, an analogous catalyst containing 3% of Au embedded on ceria and catalysts containing 1 and 3% of Au obtained by an optimized Deposition Precipitation with Urea (DPU) have also been investigated. The use of DPU as "reference" materials is based on evidence that it leads to good Au dispersions and highly active Au-based catalysts, together with the advantage of obtaining a complete deposition of Au on the support.[37,38]

Experimental Section

Materials. Hydrogen tetrachloroaurate(III) (99.999%), ammonium cerium(IV) nitrate ($(NH_4)_2Ce(NO_3)_6$, CAN, (99.99%), 16-mercaptohexadecanoic acid, 16-MHA (90%), and $NaBH_4$ (≥98%) were purchased from Sigma-Aldrich. Hexamethylenetetramine, $(CH_2)_6N_3$, (99.5%) was purchased from Analyticals. Deuterated solvents were purchased from Aldrich and used as received. Dry solvents were obtained from Fluka. Chlorinated solvents were stirred over K_2CO_3 for at least 24 h prior to use. All other solvents were reagent grade and used as received.

Synthesis of MPC-C8-TEG. The synthesis of these NPs was carried out as previously described[39] using 223 mg of hydrogen tetrachloroaurate and 364 mg of HS-C8-TEG (2 mol vs Au). The reduction was carried out at 0 °C by fast addition of 242 mg of $NaBH_4$ (10 mol vs Au) dissolved in 15 mL of bidistilled water. Pure MPC-C8-TEG were obtained as brown solid, 243 mg.

^{1}H NMR, δ: 1.3 (CH_2); 1.6 (CH_2); 2.1 (CH_2CO); 3.3 (CH_3O); 3.6 (CH_2O); 3.7(CH_2O). TEM: average diameter = 1.6 nm; σ = 0.2 nm; n = 282. Estimated average composition: $Au_{140}(S\text{-}C8\text{-}TEG)_{53}$.

Synthesis of MMPC-C8-TEG/16-MHA. MPC-C8-TEG (40 mg) was dissolved in 40 mL of deoxygenated methanol, under an argon atmosphere. A solution of 3.2 mg (0.011 mmol, 0.25 equiv with respect to the thiolates forming the monolayer) of 16-MHA in 1 mL of deoxygenated methanol was added, and the mixture was kept at 28 °C for 24 h. The solvent was removed under reduced pressure, and the Au NPs were repeatedly washed with diethyl ether and centrifuged at 4000 rpm. A 41 mg portion of NPs was obtained as a brown solid. TEM: average diameter = 1.7 nm; σ = 0.3 nm; n = 421.

Preparation of 1 wt % Au@CeO_2 Catalyst. Ammonium cerium(IV) nitrate (7.5 g, 13.7 mmol) and hexamethylenetetramine (19.1 g, 0.137 mol) were dissolved into 176 mL of water and 58 mL of methanol. A solution of 40 mg of MMPC-C8-TEG/16-MHA dissolved in 40 mL of a mixture water/methanol 3/1 was added to the reaction mixture. After stirring at room temperature (RT) for 1 h, the solution was heated under reflux for 18 h. After cooling to RT, the precipitate was filtered and washed with 500 mL of water. The solid material was dried at 120 °C overnight, ground to 180 μm, and finally calcined in air for 5 h at 500 °C using a heating ramp of 3 °C min^{-1}.

Preparation of 3 wt % Au@CeO_2 Catalyst. The preparation of this catalyst followed the same procedure described above for the 1 wt % Au@CeO_2 catalyst using 120 mg of MMPC-C8-TEG/16-MHA.

Preparation of 1 wt % Au/CeO_2 by DPU Method. To a suspension of 1 g of CeO_2 (prepared as for the embedded catalyst) into 50 mL of water a solution of 20 mg of $HAuCl_4$ (0.06 mmol) and 2.52 g of urea (42 mmol) in 50 mL of water was added. The mixture, slightly acidic (pH ∼5), was stirred 1 h at RT and at 80 °C for 4 h. After cooling to RT, the precipitate was collected by centrifugation and washed three times with water-isopropanol 1:1, then with water until no chlorides were found in the mother liquors. The product was finally dried at 120 °C overnight, ground to 180 μm, and calcined in air for 5 h at 300 °C using a heating ramp of 3 °C min^{-1}.

Preparation of 3 wt % Au/CeO_2 by DPU Method. The preparation of this catalyst followed the same procedure described above for the 1 wt % Au/CeO_2 using 62 mg of $HAuCl_4$.

PROX Experiments. All catalytic tests were conducted at atmospheric pressure. The fresh catalysts were pretreated in a flowing mixture of 5% O_2−95% Ar at 40 mL min^{-1} for 30 min at 250 °C (DPU samples) or 450 °C (embedded samples), after heating from RT at 10 °C min^{-1}. No other activation procedures were applied. Typically ∼48 mg of fresh sample were positioned in a U-shaped, quartz microreactor with internal diameter of 4 mm. The total gas flow rate under reaction conditions was 60 mL min^{-1} to ensure a Gas Hourly Space Velocity (GHSV) of ∼75000 mL g^{-1} h^{-1}. The feed gas was 1.0 vol % CO, 1.0 vol % O_2, 47.5 vol % H_2, 17.5 vol % CO_2, and 5.0 vol % H_2O in Ar. This gaseous mixture was introduced in the reactor at 75 °C. All heating and cooling rates were 2 °C min^{-1} unless otherwise noted. An aging/reactivation protocol was used to test the thermal stability of the materials prepared and is as follows:

- a first aging treatment was performed by heating the sample in the PROX environment at 150 °C and holding it at this temperature for 16 h. These samples are denoted as Aged150;
- a second aging treatment was performed taking the sample at 250 °C for 20 h. These samples are denoted as Aged250;
- a reactivation step was done by heating the sample in flowing mixture of 5% O_2−95% Ar at 40 mL min^{-1} for 30 min at 450 °C using heating and cooling rates of 10 °C min^{-1}; then the catalytic activity was measured again in the PROX mixture from 75 to 250 °C. These samples are denoted as TPO.

Reactants and products were analyzed using a mass spectrometer (Hyden Analytical HPR20) with acquisition time of the order of 1 point every 12 s. CO conversion was calculated on the basis of the decrease in the m/z 28 signal corrected for the CO_2 cracking pattern. The reaction rates were calculated based on a differential reactor from the data corresponding to % conversion

(37) Gomez-Cortes, A.; Diaz, G.; Zanella, R.; Ramirez, H.; Santiago, P.; Saniger, J. M. *J. Phys. Chem. C* **2009**, *113*, 9710.
(38) Zanella, R.; Giorgio, S.; Henry, C. R.; Louis, C. *J. Phys. Chem. B* **2002**, *106*, 7634.
(39) Pengo, P.; Polizzi, S.; Battagliarin, M.; Pasquato, L.; Scrimin, P. *J. Mater. Chem.* **2003**, *13*, 2471.

of CO below 15%. The number of accessible Au atoms were calculated on the basis of the CO chemisorptions data (see below).

Characterization Techniques. NMR spectra were recorded on a Jeol GX-400 MHz (operating at 400 MHz for ^{1}H) using $CDCl_3$ as deuterated solvent. ^{1}H NMR spectra were referenced to the residual protons in the deuterated solvent. Data are reported as follows: chemical shifts are in ppm in the δ scale; integration; assignment.

TEM images of Au NPs were obtained with a Jeol 3010 high resolution electron microscope (0.17 nm point-to-point) operating at 300 keV using a Gatan slow-scan CCD camera (mod. 794). TEM samples of protected gold NPs were prepared by placing a single drop of 0.5 mg/mL isopropanol dispersion onto a 200-mesh copper grid coated with an amorphous carbon film. The grid was then dried in air for 24 h. Depending on the Au core size, magnifications between 250000 and 600000 were used for counting purposes. Diameters were measured manually using Gatan software Digital Micrograph (ver. 3.4.1) on at least 250 particles.

N_2 physisorption and CO chemisorption experiments were carried out on a Micromeritics ASAP 2020C. The samples were first degassed in vacuum at 250 °C (for DPU catalysts) or 350 °C (for embedded samples) overnight prior to N_2 adsorption at the liquid nitrogen temperature. CO adsorption experiments were conducted at RT in the pressure range 1 to 400 Torr. Adsorption values were obtained by linear extrapolation to zero pressure of the second adsorption isotherm, as proposed by Collins et al.[40] Before CO chemisorption, the fresh samples were cleaned in flowing 5% O_2−95% Ar at 250 °C for 1 h and then evacuated at the same temperature for 1 h while the aged samples were subjected only to the evacuation pretreatment.

Powder X-ray diffraction patterns were collected on a Philips PW 1710/01 instrument with CuK_α radiation (graphite monochromator). Diffraction patterns were taken with a 0.02 degree step size, using a counting time of 10 s per point.

Before each temperature programmed reduction (TPR) experiment, the samples were pretreated in flowing 5% O_2−95% Ar mixtures at 250 °C (DPU samples) or 450 °C (embedded samples). The measurements were performed in a conventional system equipped with a thermal conductivity detector (TCD),[41] under 5% H_2−95% Ar mixtures, using a gas flow rate of 25 mL min^{-1} and a heating rate of 10 °C min^{-1}.

EXAFS and XANES spectra were recorded at the SAMBA beamline of the SOLEIL synchrotron radiation center (France). Harmonic rejection was obtained by using two Pd-coated Si mirrors, whereas the sagittaly focusing Si (220) monochromator was operated fully tuned. Measurements were performed in the fluorescence mode at liquid nitrogen temperature; beam intensity was measured before and after samples and reference foils by ionization chambers. EXAFS spectra were recorded at the L_{III} edge of Au (11019 eV). An Al filter was located at the entrance of the fluorescence detector to reduce L edge Ce fluorescence. Samples were prepared by dilution in BN after grinding the powders in an agate mortar, and pressed into pellets. Data analysis was performed with the Ifeffit code[42,43] using theoretical standards calculated with Feff 8.[44,45] Data fitting in r-space was extended up to 0.4 nm.

Images of the samples were acquired also by the HAADF method in STEM mode with a 200 kV JEOL JEM-2100F aberration corrected TEM/STEM instrument, with a probe size of better than 0.104 nm at full-width half-maximum and a collection semiangle in the range of 80−210 mrad.

Results and Discussion

Design and Synthesis of Au@CeO_2 Catalyst. The design of the embedded Au@CeO_2 catalysts was based on the use of monolayer protected gold NPs. This approach is very flexible as (i) it enables a precise control of dimension and dispersion of gold NPs and, in particular, to have rather small NPs with an average diameter lower than 2 nm; (ii) it can exploit the protective monolayer to insert appropriate functional groups, on the monolayer surface, to favor the growth of the inorganic oxide around the NPs. In principle, this approach guarantees a good metal/support interaction, limiting the merging of Au NPs and sintering at high temperature. To this aim carboxylic groups have been introduced on the surface of protected gold NPs soluble in water. Indeed, it is known that cerium hydroxide forms covalent bond with carboxylate groups.

Specifically we attempted the encapsulation of preformed Au NPs into a porous CeO_2 surrounding layer. The preparation of Au@CeO_2 catalysts comprised three main steps (Figure 1): (i) synthesis of mixed-monolayer protected Au NPs; (ii) self-assembly assisted precipitation of $Ce(OH)_x$ around the preformed Au NPs; (iii) calcination to remove organics and to obtain the Au@CeO_2 structures.

Water-soluble gold NPs protected by an amphiphilic thiol (MPC-C8-TEG) were employed. The thiol (HS-C8-TEG) is characterized by an alkyl chain of seven methylene groups close to the sulfur to completely passivate the gold surface, and a short triethyleneglycol monomethyl ether moiety to impart solubility in water.[39] The reaction conditions enable us to obtain Au NPs with an average diameter of the gold core of 1.6 nm as determined by TEM analysis. An average composition of Au_{140}(S-C8-TEG)$_{53}$ was estimated by comparison with MPC-C8-TEG of same size previously synthesized and analyzed by TEM and TGA (ThermoGravimetric Analysis).[46] The monolayer was functionalized by place exchange reaction following the procedure reported by Murray and co-workers to introduce a thiol presenting a terminal carboxylic group, 16-mercaptohexadecanoic acid (16-MHA).[47] The length of this thiol ensures that carboxylic groups stretch out of the monolayer to interact efficiently with the ceria precursor and define the size of the cavities in the ceria framework. The presence of 16-MHA contributes to a monolayer thickness of about 2 nm and thus to increase the core diameter up to 5−6 nm determining the final ceria network curvature.

(40) Collins, S. E.; Cies, J. M.; Del Rio, E.; Lopez-Haro, M.; Trasobares, S.; Calvino, J. J.; Pintado, J. M.; Bernal, S. *J. Phys. Chem. C* **2007**, *111*, 14371.
(41) Fornasiero, P.; Dimonte, R.; Rao, G. R.; Kaspar, J.; Meriani, S.; Trovarelli, A.; Graziani, M. *J. Catal.* **1995**, *151*, 168.
(42) Ravel, B.; Newville, M. *J. Synchrotron Radiat.* **2005**, *12*, 537.
(43) Newville, M. *J. Synchrotron Radiat.* **2001**, *8*, 322.
(44) Ankudinov, A. L.; Ravel, B.; Rehr, J. J.; Conradson, S. D. *Phys. Rev. B* **1998**, *58*, 7565.
(45) Rehr, J. J.; Kas, J. J.; Prange, M. P.; Sorini, A. P.; Takimoto, Y.; Vila, F. *C. R. Phys.* **2009**, *10*, 548.
(46) Lucarini, M.; Franchi, P.; Pedulli, G. F.; Gentilini, C.; Polizzi, S.; Pengo, P.; Scrimin, P.; Pasquato, L. *J. Am. Chem. Soc.* **2005**, *127*, 16384.
(47) Hostetler, M. J.; Green, S. J.; Stokes, J. J.; Murray, R. W. *J. Am. Chem. Soc.* **1996**, *118*, 4212.

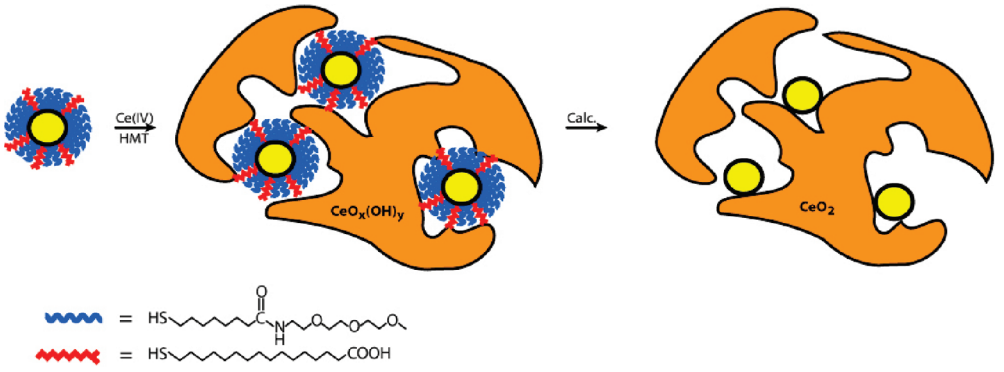

Figure 1. Schematic representation of the preparation method to obtain Au@CeO_2 catalysts.

Preliminary experiments showed that precipitation of $Ce(OH)_x$ with the commonly used urea method[48] was incomplete or, using large excess of that reagent, led to low surface area materials, which are intrinsically useless in catalysis. Therefore, hexamethylenetetramine was used as precipitating agent. In fact, under heating this compound decomposes to ammonia and formaldehyde, leading to a slow increase in the pH and, thus, to a slow precipitation of $Ce(OH)_x$.[49] The precipitation conditions were optimized to fully precipitate the cerium ions present in solution and to control the porosity of the final material. During calcination, the organic component is removed and $Ce(OH)_x$ is converted into CeO_2, ideally leading to a 3-dimensional network of Au particles embedded into the porous support. The size of the pores is extremely important, as it can limit the accessibility to the active phase and/or induce diffusion limitations. The pores must be sufficiently narrow to reduce the mobility of gold NPs, preventing the deactivation due to sintering phenomena, but sufficiently large to favor the accessibility of the reactants to the metal. Furthermore, the pores structure of the material must be sufficiently stable to cope with the working conditions of the catalyst. The calcination conditions (500 °C in air) were chosen as the lowest temperature to form CeO_2 from the $Ce(OH)_x$ precursor and to avoid unwanted sintering.

Synthesis of Au/CeO_2 by DPU. The preparation of 1 and 3 wt % Au/CeO_2 catalysts by Deposition Precipitation with Urea (DPU) was carried out following the optimized method developed by Zanella et al.[38] Briefly, an aqueous suspension of ceria, prepared as above-reported for the embedded catalyst, containing tetrachloroauric acid and a large excess of urea was warmed up at 80 °C for 4 h to hydrolyze the urea and to deposit $Au(OH)_3$ on the ceria surface. The product was then dried at 120 °C and calcined at 300 °C for 5 h.

Catalytic Activity under PROX Conditions. Figure 2 reports the catalytic activity under real PROX conditions (presence of CO_2 and water) for the 1 and 3 wt % DPU and embedded samples. The Au(1%)/CeO_2-DPU catalyst shows a modest activity as it reaches 40% CO conversion only at ~160 °C (Figure 2A). Moderate but appreciable and progressive deactivation occurs upon steady state activity at relatively low temperatures (150 and 250 °C), with light-off curves spread onto a large range of temperatures. A mild regenerative oxidative treatment is able to recover only partially the initial activity. The activity of the Au(3%)/CeO_2-DPU sample (Figure 2B) shows better CO conversion at lower temperature, consistently with the higher Au loading in association with a good initial metal dispersion (see below). However, also in this case a progressive deactivation is observed and the initial activity is not completely retrieved after a mild oxidative treatment.

The performance of the embedded Au(1%)@CeO_2 catalyst is reported in Figure 2C. This material is much more active than the reference Au(1%)/CeO_2-DPU catalyst, reaching the maximum CO conversion (~65%) at ~130 °C. The low activity at moderate temperatures (< 100 °C) could mainly be due to the strong adsorption of water on the active sites.[50] However, the presence of moisture has a positive effect at temperatures higher than 100 °C, as it can mediate the activation of the O_2 molecule by OH groups deriving from water adsorption on the support surface.[51] In addition, Au/CeO_2 systems are good low-temperature Water-Gas Shift-Reaction (WGSR) catalysts,[10,52] and this reaction can account for an additional CO removal at increasing temperatures. The presence of water has also proved to contribute in the desorption of surface carbonates, which are well-known poisoning byproducts for CeO_2.[53,54] For comparison, the activity of the 3 wt % embedded catalyst is reported in Figure 2D. Contrary to what is observed for the DPU samples, the activity is not significantly affected by the Au loading. This might suggest that, in the presence of a relatively high Au loading, the fraction of completely buried Au particles inside the support could be significant and thus inaccessible to the reactants or that larger Au particles are present. Both embedded catalysts moderately deactivate after the aging treatments at 150 and 250 °C, as in the case of the DPU samples. However, while the activity of

(48) Li, Y.; Fu, Q.; Flytzani-Stephanopoulos, M. *Appl. Catal., B* **2000**, *27*, 179.
(49) Polezhaeva, O. S.; Yaroshinskaya, N. V.; Ivanov, V. K. *Inorg. Mater.* **2008**, *44*, 51.
(50) Date, M.; Haruta, M. *J. Catal.* **2001**, *201*, 221.
(51) Date, M.; Ichihashi, Y.; Yamashita, T.; Chiorino, A.; Boccuzzi, F.; Haruta, M. *Catal. Today* **2002**, *72*, 89.
(52) Fu, Q.; Deng, W.; Saltsburg, H.; Flytzani-Stephanopoulos, M. *Appl. Catal., B* **2005**, *56*, 57.
(53) Karpenko, A.; Leppelt, R.; Plzak, V.; Cai, J.; Chuvilin, A.; Schumacher, B.; Kaiser, U.; Behm, R. J. *Top. Catal.* **2007**, *44*, 183.
(54) Kim, C. H.; Thompson, L. T. *J. Catal.* **2005**, *230*, 66.

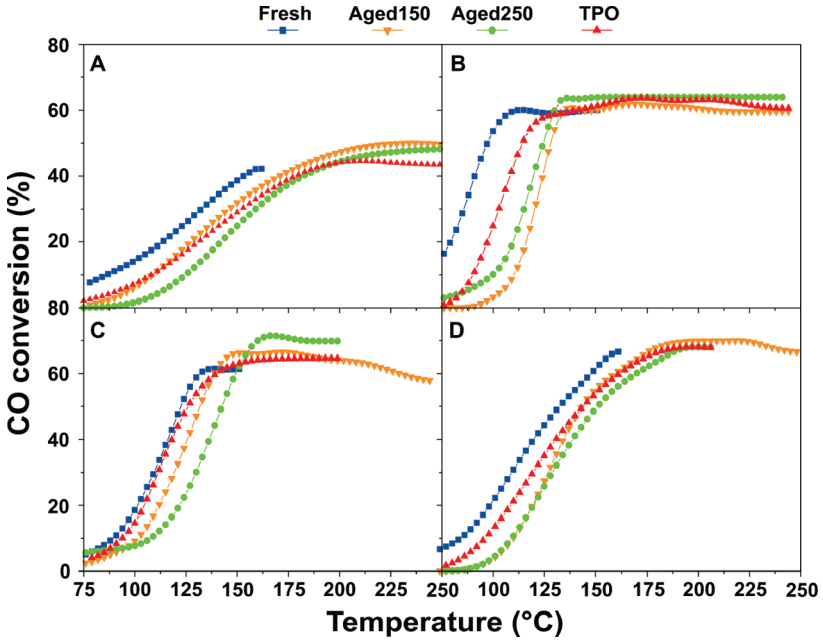

Figure 2. Catalytic activity of: Au(1%)/CeO_2-DPU (A); Au(3%)/CeO_2-DPU (B); Au(1%)@CeO_2 (C); Au(3%)@CeO_2 (D). PROX conditions: CO(1.0%) + O_2(1.0%) + H_2(47.5%) + CO_2(17.5%) + H_2O (5.0%), balance Ar; GHSV = 75000 mL g^{-1} h^{-1}. Consecutive catalyst treatments: Fresh (after calcination); Aged150 (after aging under reaction conditions at 150 °C for 16 h); Aged250 (after aging under reaction conditions at 250 °C for 20 h); TPO (after treatment in O_2/Ar at 450 °C for 30 min).

the DPU samples can be restored only partially by the mild oxidative treatment, the embedded catalysts fully recover their initial activity following the same treatment. Experiments carried out in the absence of water (not reported) show a more prominent deactivation, confirming that water has a positive effect in removing carbonate species that block the active sites. Notably, the light-off curves of the embedded catalyst are quite sharp while those of the DPU sample are rather flat. This can be interpreted as an indirect indication that the embedded catalyst possesses a more homogeneous distribution of the active phase. This is in agreement with the goal of our preparation strategy which is based on the use of preformed gold NPs with a narrow size distribution.

The nature of the PROX active sites has been largely debated in the literature and many reports indicate a key role of the metal−support interface perimeter.[25,55−57] In particular, it has been suggested that oxygen vacancies on the ceria surface and close to gold clusters promote CO oxidation.[58,59] Consistently, the reactivity and the electronic and structural features of oxidized Au-Ceria based sample differ from that of the corresponding pre-reduced materials.[60,61] However, under operative steady state PROX conditions, the simultaneous presence of large quantity of hydrogen, water, and CO_2 leads to the establishment of an equilibrium between Ce(III) and Ce(IV). Temperature Programmed Reduction experiments (see below) confirm that surface cerium can be partially reduced above 70 °C in both the embedded and the DPU samples, suggesting a role of the oxygen vacancies in the PROX mechanism.

Finally, selectivity is an important catalyst feature. O_2 selectivities for all the investigated catalysts are almost constant during the experiments with a value of about 40% (i.e., full oxygen consumption is observed at the maximum CO conversion). This is a value in line with PROX behavior of most of Au-based catalysts.[9,10]

The activities of the fresh catalysts were also expressed in terms of turnover frequencies calculated on the basis of the accessible Au atoms, measured through CO chemisorption (see below), and the kinetic parameters of CO oxidation under real PROX conditions were calculated and listed in Table 1.

TOFs values (Table 1) were calculated from the run up experiments of Figure 2 from conversion data below 15%. Selected steady state experiments on Au(1%)@CeO_2 showed that small but progressive deactivation was observed even at 80 °C. A loss of 2% conversion was estimated within 5 h of reaction. This is due to the unavoidable formation of carbonates. Consistently the same deactivation effect was marginal when CO_2 was not present in the gas feed (data not shown). In fact, in this latter case the low CO conversion and the diluted conditions prevent significant formation of carbonate. In the case of Au(1%)/CeO_2-DPU sample, a very similar deactivation phenomenon was observed indicating that at low temperature (80 °C) the Au sintering, if present, proceeds rather slowly. This latter effect, being temperature dependent, becomes certainly significant at higher temperature, where CO conversion becomes more important. Conversions (Figure 2) and TOFs (Table 1) data are an indication that our Au embedded

(55) Bond, G. C.; Thompson, D. T. *Catal. Rev.* **1999**, *41*, 319.
(56) Hutchings, G. J. *Gold Bull.* **2004**, *37*, 3.
(57) Bond, G. C.; Louis, C.; Thompson, D. T. *Catalysis by Gold*; Imperial College Press: London, 2006.
(58) Shapovalov, V.; Metiu, H. *J. Catal.* **2007**, *245*, 205.
(59) Widmann, D.; Leppelt, R.; Behm, R. J. *J. Catal.* **2007**, *251*, 437.
(60) Manzoli, M.; Boccuzzi, F.; Chiorino, A.; Vindigni, F.; Deng, W.; Flytzani-Stephanopoulos, M. *J. Catal.* **2007**, *245*, 308.
(61) Avgouropoulos, G.; Manzoli, M.; Boccuzzi, F.; Tabakova, T.; Papavasiliou, J.; Ioannides, T.; Idakiev, V. *J. Catal.* **2008**, *256*, 237.

Table 1. Kinetic Parameters for CO Conversion under Real PROX Conditions

catalyst	D_{metal}[a] (nm)	$T_{1/2}$[b] (°C)	TOF at 80 °C (s^{-1})	TOF at 95 °C (s^{-1})
CeO_2	-	250[c]	0	0
Au(1%)@CeO_2	< 1.0	110	3.2×10^{-2}	4.3×10^{-2}
Au(1%)/CeO_2-DPU	2.0 ± 0.6	159[d]	2.5×10^{-2}	4.0×10^{-2}
Au(3%)@CeO_2	1.3 ± 0.2	113	3.6×10^{-2}	8.0×10^{-2}
Au(3%)/CeO_2-DPU	2.4 ± 0.4	97	2.6×10^{-2}	-

[a] As determined by EXAFS. [b] Temperature for 50% CO conversion of fresh catalysts under real PROX conditions. [c] CO conversion of bare CeO_2 was negligible up to 250 °C. [d] CO conversion at 159 °C was 42%.

catalysts possess a promising activity, that could be further improved, and prove the absence of significant drawbacks of dramatic metal encapsulation effects.

Characterization of the Catalysts

Textural Properties. N_2 adsorption isotherms and pore size distributions of the samples are reported in Figure S1 (Supporting Information). All materials show type IV isotherms, which are typical of mesoporous systems. The isotherms are very similar in shape, while minor differences in total pore volume and surface area can be appreciated (Table T1, Supporting Information). The form of the hysteresis loop of the adsorption isotherms suggests that the pores of all the investigated materials have an "ink-bottle" shape, with a narrower opening and a larger bottom. The pore distribution shows a very narrow dispersion, with dimensions of the openings less than 5 nm and a maximum centered at 4 nm. About 90% of the total volume is originated by pores of openings less than 5 nm. Physisorption data on samples that have been tested under reaction conditions at 150 and 250 °C (Aged250) evidence that only a slight decrease in the Brunauer−Emmett−Teller (BET) surface area is observed after the aging treatments (Table T1, Supporting Information). This result is an indication of the good thermal stability of the support.

X-ray Diffraction (XRD). Powder XRD patterns of the catalysts are dominated by the reflections originated by fluoritic CeO_2. (Figure S2, Supporting Information). The mean crystallite size, calculated applying Scherrer's equation to the (111) reflection of CeO_2, is 8 nm for all samples, even after aging at 250 °C. These data are in good agreement with the HAADF-STEM observations of the catalysts (see below). XRD reflections attributable to Au phases were not observed in the 1% Au samples because of the very low metal loading and the small Au particle size. In fact, the XRD pattern of fresh Au(1%)@CeO_2 sample is essentially equivalent to that of the bare support, with slight differences in the width of the reflections because of the lower surface area of the catalyst. In the case of 3 wt % Au loaded samples, both fresh samples show only a small and broad reflection corresponding to Au (111) at 38.4° (insets of Supporting Information, Figure S2). This indicates that the crystallites are very small. The aging treatments do not significantly influence the XRD patterns of the catalysts.

Temperature-Programmed Reduction (TPR) Experiments. TPR experiments were used to study the influence of gold on CeO_2 reducibility. Supporting Information, Figure S3 shows both high-temperature (top) and low-temperature (bottom) TPR profiles recorded for CeO_2 support and fresh Au(1%)@CeO_2 and Au(1%)/CeO_2-DPU catalysts.

The bare support shows two reduction peaks: one at lower temperature (~520 °C) assigned to surface capping oxygen and a second at higher temperature (~800 °C), because of lattice oxygen removal, in accordance with the literature.[30] With the limitations due to the correct baseline subtraction and the contribution of a negative-desorption peak, a total uptake of ~1340 μmol H_2 g^{-1} was calculated using CuO as standard, suggesting that ~46% of the cerium is reduced to Ce(III) during TPR.

Embedded and DPU catalysts show the high-temperature reduction peak in the same range of the bare support (~800 °C) even if its intensity is reduced (~35% of the H_2 consumption of the bare support). Exact quantification of the total hydrogen consumption is complicated by the fact that some reduction occurs at RT, especially in the case of DPU sample. As a general comment, the total amount of hydrogen uptake during TPR appears to be only marginally increased with respect to the bare support. The low-temperature Ce(IV) to Ce(III) reduction peak shifts at lower temperatures because of the presence of Au, which weakens the surface oxygen of CeO_2.[11] The shift of the surface reduction peak of CeO_2 to lower temperature is a common issue observed when noble metals are deposited onto this support.[62,63] This is an indirect indication that the DPU method leads to a homogeneously dispersed Au phase. Vice versa, in the TPR of the embedded catalyst, in addition to the above-mentioned reduction processes, there is an hydrogen uptake at intermediate temperature (485 °C). This suggests the presence of some CeO_2 grains which are not in contact with the metal. Even in this case, the hydrogen uptake due to the high temperature bulk reduction of ceria is significantly reduced (~45% of the H_2 consumption of the bare support). The hydrogen uptake below RT (Supporting Information, Figure S4, bottom part) for the metal loaded catalysts could be associated with the titration of oxygen adsorbed onto the surface of small Au clusters.[64]

Chemisorption of CO. Despite that there is a debate about the ability of Au to dissociate and chemisorb H_2, Au chemisorbs CO, even if weakly. However, in the case of Au-CeO_2 systems, the support chemisorbs CO stronger than Au, forming surface carbonates. This problem has

(62) Trovarelli, A.; Dolcetti, G.; de Leitenburg, C.; Kaspar, J.; Finetti, P.; Santoni, A. *J. Chem. Soc., Faraday Trans.* **1992**, *88*, 1311.
(63) Hickey, N.; Fornasiero, P.; Kaspar, J.; Gatica, J. M.; Bernal, S. *J. Catal.* **2001**, *200*, 181.
(64) Boccuzzi, F.; Chiorino, A.; Manzoli, M.; Lu, P.; Akita, T.; Ichikawa, S.; Haruta, M. *J. Catal.* **2001**, *202*, 256.

been recently addressed by Collins et al., who defined a procedure to estimate Au dispersion in $Au/Ce_xZr_{1-x}O_2$ samples.[40] The accessible Au sites of our catalysts were obtained following their approach, and the results are reported in Table 2.

DPU samples show very good Au accessibilities, 51 and 41% for 1 and 3 wt % samples, respectively. This indicates that about half of the Au atoms are able to interact with CO and coordinate it. The good capability of CO chemisorption is in line with the expectation for the reference samples prepared by the DPU method. In fact, their preparation was optimized to obtain highly dispersed Au NPs onto the surface of the support. The higher metal accessibility of the 1 wt % DPU sample suggests that the increase of metal loading has a negative effect. During both the synthesis and the calcination step, there is a higher probability of metal merging to form larger particles. In the case of Aged250 samples, the Au accessibilities drop by a significant extent (from 51 to 16% and from 41 to 11% for 1 and 3 wt % Au, respectively). This can be due to the concomitant blockage of Au sites by carbonate-like deposits, as observed using IR spectroscopy on Aged250 samples (bands at 1300−1400 cm^{-1},[54] Supporting Information, Figure S4), and to the occurrence of sintering. Following the reactivation by TPO, the Au accessibility of the 1% DPU catalyst significantly increases leading to an apparent metal dispersion of 93% (Table 2). The reason of this remarkable change is related to the nature of the present materials. In particular, this catalyst was initially calcined only at 300 °C, temperature reported as sufficient to remove organic residues from the synthesis[38] and low enough to preserve the desired high metal dispersion. The reactivation of the aged sample was performed at 450 °C. During this treatment, an appreciable oxygen uptake at 450 °C and a very small concomitant CO_2 and NO_x evolution was observed. This suggests the presence of only few traces of residues from the synthesis. Therefore, the activity and metal accessibility of the fresh 1% DPU sample could have in part been reduced by the presence of traces of synthesis residues, which partially cover the metal surface or contribute to occlude some pores of the catalyst. In addition, the oxygen uptake during the mild regenerative treatment could suggest the presence of some Ce(III) as previously observed for small CeO_2 NPs.[65] Electronic deactivation of the chemisorption capability of various metals was previously observed in reduced ceria based systems.[66] The relatively more severe oxidation treatment during the TPO (450 °C) with respect to the initial calcination process (300 °C) can annihilate any eventual presence of traces of Ce(III) and therefore the negative electronic influence. Finally, the increase in the Au accessibility can be related mainly to a redispersion of the metal phase after the treatment in oxygen, as already reported for Pd.[67] Nevertheless, the activity of this catalyst aged under PROX conditions is not recovered after TPO treatment. This reveals that not only a metal redispersion occurs but also a reorganization of the catalytic active sites is induced by the mild oxidation treatment. Furthermore, the degree of this reconstruction strongly depends on the history of the materials. In fact, the sintering extent is related to the thermo-chemical conditions applied, reducing conditions being more effective than those oxidizing, such as the calcination step.[68,69] Consistently, by applying the regenerative mild oxidation treatment on the fresh 1 wt % Au/CeO_2 DPU catalyst, a promotion of the initial catalytic activity (Supporting Information, Figure S5) with respect to the fresh sample and higher metal accessibility (74 vs 51%) were observed. Therefore, after a severe sintering leading to an average overtake of a critical Au particle diameter, the metal redispersion results unfavorable. In the case of the 3 wt % DPU catalyst, the reactivation does not lead to a complete recovery of the Au accessibility, which reaches a final value of 34%. This is in accordance with the partial reactivation of the catalyst after mild oxidation treatment, suggesting that sintering of Au occurred in this sample.

Table 2. CO Chemisorption Results on Au/CeO_2 Catalysts after Different Treatments[a]

sample	treatment	accessible Au sites[b]	accessible Au surface ($m^2\ g^{-1}$)
$Au(1\%)@CeO_2$	Fresh	31%	0.96
	Aged250	29%	0.89
	TPO	34%	1.06
$Au(1\%)/CeO_2$-DPU	Fresh	51%	1.57
	Aged250	16%	0.49
	TPO	93%	2.85
$Au(3\%)@CeO_2$	Fresh	10%	0.96
	Aged250	7%	0.66
	TPO	25%	2.30
$Au(3\%)/CeO_2$-DPU	Fresh	41%	3.80
	Aged250	11%	1.03
	TPO	34%	3.19

[a] Fresh (after calcination); Aged250 (after aging under reaction conditions at 150 °C for 16 h and at 250 °C for 20 h); TPO (after treatment in O_2/Ar at 450 °C for 30 minutes). [b] Assuming a CO/Au stoichiometric ratio of 0.33.[40]

On the other hand, the fresh embedded catalysts show lower Au accessibilities (31 and 10% for 1 and 3% catalysts, respectively). Taking into account that XAS highlighted the presence of very small particles in the catalysts (see below), the lower Au accessibility in these samples can be interpreted assuming that a significant portion of the metal is fully buried into the CeO_2 support and thus not available to CO. Despite this fact, the good catalytic activity indicates that the fraction of accessible Au is very active. This could be related to the fact that nanocrystalline CeO_2 can enhance the formation of reactive O_2 species,[18,70] and the larger contact area between Au and CeO_2 in the embedded sample with respect to the DPU sample can account for its higher activity. After the aging treatments,

(65) Dutta, P.; Pal, S.; Seehra, M. S.; Shi, Y.; Eyring, E. M.; Ernst, R. D. *Chem. Mater.* **2006**, *18*, 5144.
(66) Bernal, S.; Calvino, J. J.; Cauqui, M. A.; Gatica, J. M.; Larese, C.; Perez Omil, J. A.; Pintado, J. M. *Catal. Today* **1999**, *50*, 175.
(67) Lieske, H.; Voelter, J. *J. Phys. Chem.* **1985**, *89*, 1841.
(68) Fornasiero, P.; Balducci, G.; Di Monte, R.; Kaspar, J.; Sergo, V.; Gubitosa, G.; Ferrero, A.; Graziani, M. *J. Catal.* **1996**, *164*, 173.
(69) Gatica, J. M.; Baker, R. T.; Fornasiero, P.; Bernal, S.; Kaspar, J. *J. Phys. Chem. B* **2001**, *105*, 1191.
(70) Guzman, J.; Carrettin, S.; Corma, A. *J. Am. Chem. Soc.* **2005**, *127*, 3286.

in both samples the Au accessibility slightly decreases (from 31 to 29% for the 1% and from 10 to 7% for the 3% embedded catalysts). Finally, after the regenerative TPO treatment, the Au accessibility is completely recovered. This is an indication that the formation of carbonates could be the main reason of deactivation on the embedded catalysts. Furthermore, since the PROX activity of the catalysts is completely retrieved, the active sites do not change during aging and TPO treatments. This evidences the robustness of the embedding approach.

HAADF-STEM. Preliminary conventional TEM and HRTEM characterization of the embedded samples failed in finding discrete Au NPs. This is due to the high electron density of ceria[71] and to the fact that Au NPs are hidden by the protective ceria layer. Therefore we tried to overcome this problem using the HAADF-STEM technique. The contrast in the images of this method is very sensitive to the atomic number Z of the element, and therefore it has more sensitivity than conventional TEM in distinguishing elements with a small Z difference. Although this difference between gold and cerium is not large, the oxide support provides enough contrast to distinguish gold NPs even when they are under a thin layer of support. The distribution and identification of the Au NPs in the ceria matrix was confirmed by EDX analysis.

Representative HAADF-STEM images of fresh and Aged250 Au(1%)@CeO_2 samples showed faceted Au NPs in the range 1−3 nm (Figures 3A and 3B) in accordance with the starting dimension of protected Au NPs. We could not rule out the presence of subnanometer particles/clusters in our samples because of the intrinsic difficulty in imaging the samples and to the effect of sample thickness (the contrast of gold clusters degrades even more in the smaller clusters sizes because the thickness decreases), as already observed in the Au/FeO_x system.[24] The presence of Au NPs in the range 1−3 nm can be appreciated even after aging; the particles are surrounded by CeO_2 crystallites. Despite the fact that completely buried Au NPs are not visible with this technique, this is a demonstration that the embedding approach successfully leads to the formation of a protective CeO_2 layer around the preformed metal particles. Remarkably, ceria appears nanostructured, with faceted crystallites of about 8−10 nm, in accordance with XRD. Ceria can be seen as bigger faceted particles with lower contrast in the STEM images.

On the other hand, representative images of fresh and Aged250 Au(1%)/CeO_2-DPU catalyst (Figures 3C and 3D) showed (i) the presence of larger particles even in the fresh catalyst; (ii) the presence of a broader size distribution of the particles; (iii) that Au NPs in this case are preferentially located at the edges of the CeO_2 crystallites, an event that was not observed in the embedded catalyst sample. We can not rule out the presence of subnanometer Au particles in this sample either. However, after

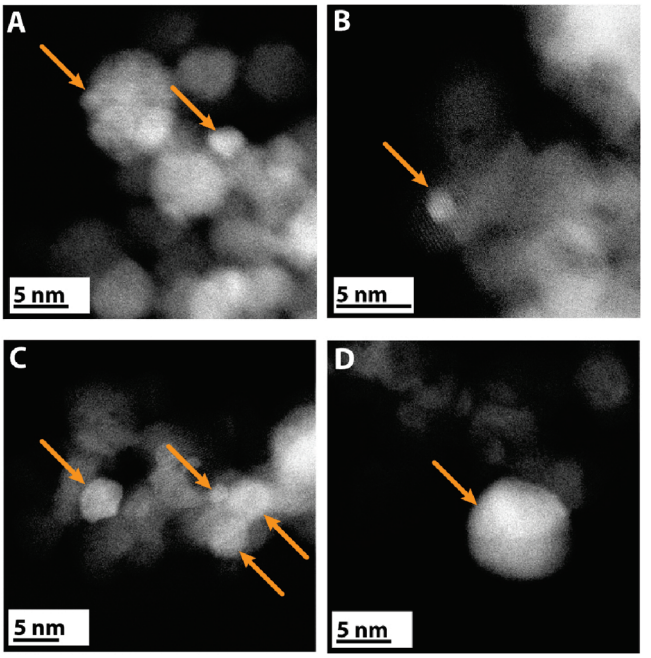

Figure 3. HAADF-STEM images of Au(1%)@CeO_2 (Fresh, A and Aged250, B) and Au(1%)/CeO_2-DPU (Fresh, C and Aged250, D) samples with faceted Au NPs evidenced by arrows.

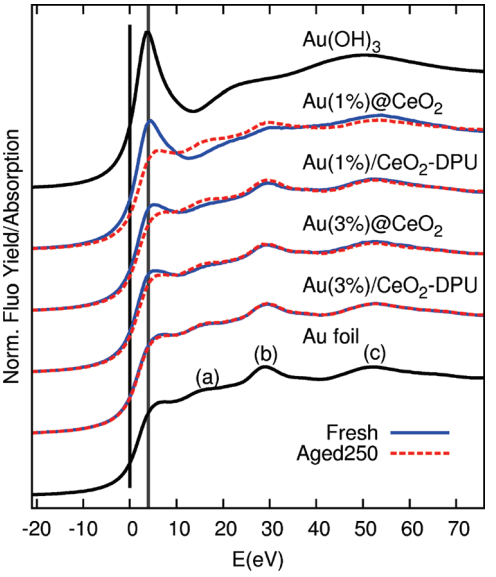

Figure 4. Au L_{III}-edge XANES spectra of the samples subjected to different treatments: Fresh (after calcination); Aged250 (after aging under reaction conditions at 150 °C for 16 h and at 250 °C for 20 h).

aging, the presence of large Au NPs (10−20 nm) in the DPU sample is a clear indication that sintering occurred in this catalyst.

Representative HAADF-STEM images of fresh and Aged250 Au(3%)@CeO_2 are reported in Supporting Information, Figure S6. In the fresh embedded sample, some large Au particles (~10 nm) are visible. This could be the result of an imperfect encapsulation of some particles, which remain on the surface of ceria. Thus, after the calcination step, they suffer of sintering. However, a more accurate analysis using aberration-corrected STEM allowed us to find also small particles (1−3 nm in dimension), which

(71) González, J. C.; Hernández, J. C.; López-Haro, M.; del Río, E.; Delgado, J. J.; Hungría, A. B.; Trasobares, S.; Bernal, S.; Midgley, P. A.; Calvino, J. J. *Angew. Chem., Int. Ed.* **2009**, *48*, 5313.

Table 3. XANES and EXAFS Data of Au/CeO_2 Catalysts[a]

sample	treatment	% Au(III)[b]	N[c]	R (nm)	D (nm)[f]
Au foil			Au x 12	0.286(1)[d]	
Au(1%)@CeO_2	Fresh	55	O x 1.9 (4)	0.197(1)[e]	< 1.0 [5.8]
			Au x 5.0(1.0)	0.286(1)[d]	
	Aged250	7	Au x 6.2(9)	0.287(1)[d]	1.0(1) [1.0]
Au(1%)/CeO_2-DPU	Fresh	21	Au x 9.0(1.0)	0.286(1)[d]	2.0(6) [8.5]
	Aged250	1	Au x 9.5(5)	0.286(1)[d]	2.3(5) [2.1]
Au(3%)@CeO_2	Fresh	18	Au x 7.8(7)	0.286(1)[d]	1.3(2) [2.0]
	Aged250	6	Au x 8.6(7)	0.286(1)[d]	1.6(3) [1.8]
Au(3%)/CeO_2-DPU	Fresh	5	Au x 9.7(4)	0.287(1)[d]	2.4(4) [2.9]
	Aged250	2	Au x 10.1(4)	0.286(1)[d]	3.0(6) [3.0]

[a] Fresh (after calcination); Aged250 (after aging under reaction conditions at 150 °C for 16 h and at 250 °C for 20 h). [b] Percentage of Au(III) content obtained by fitting XANES ± 5%. [c] Au−Au coordination number. [d] Au−Au bond distance. [e] Au−O bond distance. [f] Average Au particle dimension, values corrected for the Au(III) fraction are in square brackets.

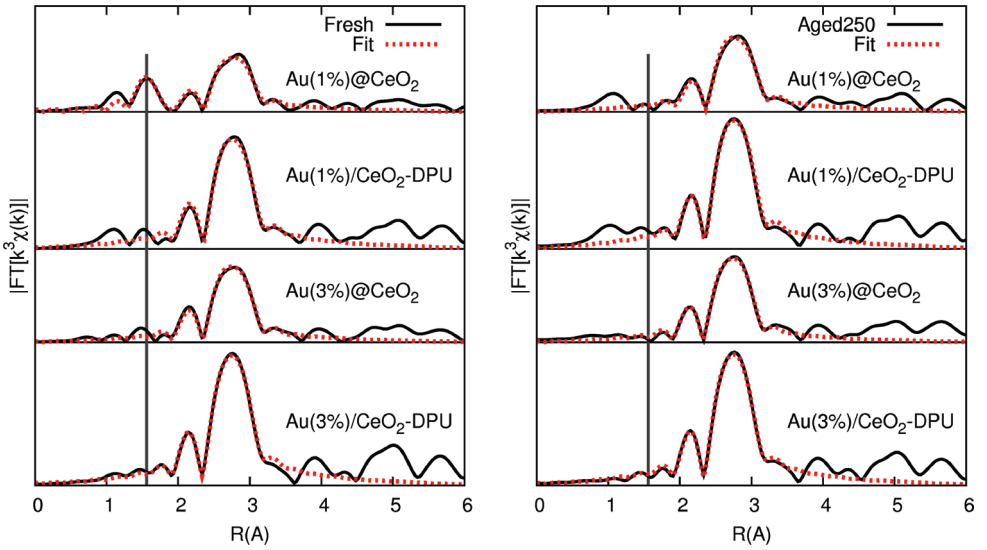

Figure 5. Au L_{III}-edge Fourier transforms of EXAFS data and fits of the samples subjected to different treatments: Fresh (after calcination); Aged250 (after aging under reaction conditions at 150 °C for 16 h and at 250 °C for 20 h).

are clearly embedded inside the ceria support. Images of the Aged250 sample, once more, evidenced the presence of large agglomerates, which are however present even in the fresh sample. Nevertheless, it is worth noting that most of the particles should be in the range 1−3 nm, given the results from XAS experiments (see next section). The overall indication is that, by increasing the amount of Au during the preparation step, an incomplete encapsulation of some particles leads to metal agglomeration.

XAS Experiments. XANES/EXAFS were employed to reveal the oxidation state of Au and to estimate average particle dimensions as complementary information to TEM and chemisorption experiments. Au L_{III}-edge XANES spectra of the samples are reported in Figure 4 as well as Au(0) and Au(III) standards. The a, b, and c letters on the Au foil profile indicate the first Au fcc characteristic EXAFS oscillations and keep the notation used by Casaletto et al.[72] for a similar case.

Comparison with the Au foil and $Au(OH)_3$ references is straightforward, since all samples keep the peaks typical of fcc gold as in the standard gold foil. Fresh samples show an enhanced first peak well corresponding to that of Au(III), 4 eV above the threshold.[72] This peak is more pronounced for lower Au loadings and for embedded particles versus the DPU prepared ones. An estimate of the relative amount of Au(III) is obtained by a linear combination of Au(0) and Au(III) standards in the XANES region, as reported in Table 3. The presence of Au(III) can be related to dispersed atoms and/or most likely to atoms at the surface of the clusters, eventually in contact with the matrix.

The reasonably good quality of the EXAFS data allowed a deeper analysis (k^2 weighted EXAFS spectra are reported in the Supporting Information, Figure S7). In Table 3, coordination numbers and distances are reported for Au−O and Au−Au pairs, while Fourier transforms of EXAFS data and fits are shown in Figure 5. Actually, the fitting has included the Au−O pair (the position is indicated by the vertical line in Figure 5) only in one case, since in all other refinements its contribution was statistically irrelevant. Thus, XANES appears much more sensitive to the presence of Au(III) than EXAFS. The Au−Au distance is constant within the experimental

(72) Casaletto, M. P.; Longo, A.; Venezia, A. M.; Martorana, A.; Prestianni, A. *Appl. Catal., A* **2006**, *302*, 309.

error, and the most relevant trend in the series is the Au−Au coordination number. The use of this number as a precise estimate of particles size is not trivial. In addition, a good approximation is obtained for spherical metal NPs with diameter smaller than 4 nm.[73] Finally, if the oxidized fraction is neglected, the particle size is underestimated since Au(III) is not seen from Au(0) or not at the same distance as Au(0)−Au(0). Correction of the coordination number for the presence of the Au(III) fraction gives the diameter values reported in squared brackets in the last column of Table 3. The apparent large average diameter calculated for fresh Au(1%)@CeO_2 and Au(1%)/CeO_2-DPU suggests the presence of a broad distribution of particle size. The presence of some large Au NPs can not be excluded, while most of them are smaller than 3 nm. In fact, these two fresh samples are mostly oxidized; whereas after aging Au(III) becomes a smaller fraction and the EXAFS analysis better estimates the actual average diameter.

The low coordination number in the Aged250 Au(1%)@CeO_2 is remarkable. It strongly suggests that the major part of the Au NPs are very small. In contrast, the PROX aging induces a significant increase of the coordination number of Aged250 Au(1%)/CeO_2-DPU. Both aged samples show negligible fraction of Au(III). The samples with 3 wt % Au loading show an increase in the coordination number with respect to the corresponding 1 wt % samples. A further very small rise is observed after aging. The presence of an appreciable Au(III) fraction in the fresh Au(3%)@CeO_2 can be considered as a strong indication of the presence of very small Au particles in this sample.

Reports on the discrepancy between Au particles dimensions estimated using STEM and EXAFS have already been reported.[74] However, consistent trends are observed using both techniques and further supported by CO adsorption analysis on the NPs size changes. Summarizing, the embedded approach leads to a large Au(III) fraction on the fresh samples, indicating the presence of smaller particles with respect to the corresponding DPU samples. Furthermore, the data here reported suggest that the embedded strategy is able to limit metal sintering.

Conclusions

We reported a new methodology to prepare Au NPs embedded into CeO_2 by using monolayer protected gold NPs presenting carboxylic groups on the surface to direct the ceria formation. Very good catalytic activity under real PROX conditions was obtained with low metal loading (1 wt %). Fresh embedded catalysts show higher TOF with respect to the corresponding materials prepared with optimized DPU method. Moreover, the small deactivation observed for the embedded Au(1%)@CeO_2 catalysts after aging at 250 °C is fully reversible upon mild oxidation treatment. This latter process is in fact able to remove unavoidable carbonate from the active sites. Vice versa, in the case of DPU samples, only a partial recovery of the activity is observed corroborating the hypothesis of appreciable metal sintering for unprotected surface Au NPs. Despite the lower accessibility of the metal phase, as highlighted by CO chemisorption, the good activity of the embedded catalysts can be ascribed to the larger extent of metal−support interaction. TPR experiments on the embedded samples suggest that a fraction of Au NPs are completely buried inside the CeO_2 layer. This suggests that further improvements can be achieved by better tuning the porosity of the support and therefore the metal accessibility. XAS analysis, and in particular XANES data on the presence of Au(III), indicates that the fresh embedded samples present a larger fraction of NPs smaller than 2 nm. STEM analysis is consistent with this picture. In addition HR-TEM indicates that the synthetic methodology here reported for the preparation of our ceria leads to a highly nanostructured oxide. This feature has been already highlighted to improve the catalytic performances.[75]

Acknowledgment. University of Trieste, ICCOM-CNR, INSTM, PRIN2007 "Sustainable processes of 2nd generation for H_2 production from renewable sources", Fondo Trieste, Fondazione CRTrieste are acknowledged for financial support. We acknowledge SOLEIL for provision of synchrotron radiation facilities, and we would like to thank the staff of the SAMBA beamline for assistance. The research leading to these results has received funding from the European Community's Seventh Framework Programme (FP7/2007-2013) under grant agreement no. 226716. NSF Grant CTS-0500511 supported the STEM analyses at UC-Davis.

Supporting Information Available: Textural data of CeO_2 and both fresh and aged Au/CeO_2 catalysts; XRD patterns of fresh and Aged250 3 wt % DPU and embedded samples, fresh Au(1%)@CeO_2 and bare CeO_2 support; high-temperature and low-temperature TPR profiles of fresh CeO_2, Au(1%)/CeO_2-DPU and Au(1%)@CeO_2; FT-IR spectrum of aged Au(1%)@CeO_2 catalyst; CO conversion in the PROX reaction over Au(1%)/CeO_2 DPU cleaned at 450 °C for 30 min before the activity; representative HAADF-STEM images of Fresh and Aged250 Au(3%)@CeO_2 catalyst; k^2 weighted EXAFS spectra at the Au L_{III} edge of the samples subjected to different treatments. This material is available free of charge via the Internet at http://pubs.acs.org.

(73) Borowski, M. *J. Phys. IV* **1997**, *7*, C2-259.
(74) Bus, E.; Miller, J. T.; van Bokhoven, J. A. *J. Phys. Chem. B* **2005**, *109*, 14581.
(75) Carrettin, S.; Concepcion, P.; Corma, A.; Lopez Nieto, J. M.; Puntes, V. F. *Angew. Chem., Int. Ed.* **2004**, *43*, 2538.